Experimental Investigation of the Properties of a Glow Discharge used as Plasma Actuator Applied to Rarefied Supersonic Flow Control around a Flat Plate

Romain Joussot and **Viviana Lago**
ICARE, CNRS, UPR 3021
1C, Avenue de la Recherche Scientifique
45071, Orléans cedex 2, France

ABSTRACT

This paper describes experimental investigations focused on the glow discharge created by a plasma actuator and used to shock wave modification over a flat plate in a Mach 2 air flow. The model is equipped with a plasma actuator composed of two electrodes. A weakly ionized plasma is created above the plate by generating a glow discharge with a negative dc potential applied to the upstream electrode. ICCD images of the discharge without and with the Mach 2 flow show the influence of the flow field on the discharge morphology. In addition, ICCD images of the modified flow revealed that when the discharge is ignited, the shock wave angle increased with the applied voltage. Thermal measurements of the flat plate surface carried out with an IR camera showed that the spatial temperature distribution is not uniform along the plate and its maximum, near the leading edge, increases with the applied voltage. Previous results showed that surface heating is responsible for roughly 50% of the shock wave angle increase, meaning that purely plasma effects must also be considered to fully explain the flow modifications observed. The focus of this paper is the study of the properties of the glow discharge to better understand the interaction between the supersonic flow and the purely plasma effects which are responsible of flow field modifications, in particular ionization degree and thermal disequilibrium upstream the model.

Index Terms — **Glow discharges, plasmas, shock waves, flow control.**

1 INTRODUCTION

OVER the past two decades, there has been considerable research into the use of plasma-based devices in flow-control applications (*i.e.*, plasma actuators), both numerically and experimentally. Many flow regimes are concerned, from low-speed subsonic airflow to hypersonic flow, including moderate-velocity subsonic, transonic, and supersonic flows. Several reviews are available for high speed flow regimes and testify to the considerable research effort into active flow control research using plasma actuators. For instance, one can refer to the work of [1-4]. In addition, the reader can refer to the works of [5-9] which concern the use of plasma actuators at low- and moderate-speed flow regimes.

Plasma actuators are extensively deployed for flow control applications because of their ability to achieve flow actuation without moving mechanical parts and with a high-bandwidth. From a general point of view, a plasma actuator is a simple electrical device based on the use of a gas discharge. A wide variety of different types of plasma actuators has been studied in the literature. Among the ones most commonly used are those based on a surface dielectric barrier discharge (dbd) with linear [10] or serrated electrode design [11], surface dbd with multiple electrodes [12], bulk direct current (dc) glow discharge [13], surface dc discharge [14], arc discharge [15], dc filamentary discharge [16], corona discharge [17], and radio frequency discharge [18], for instance. The main limitation in using a particular type of plasma actuator is often driven by the flow conditions, especially by the pressure condition. In rarefied flow regimes, corona and glow discharges are mainly used as this regime implies low pressures.

Flow control research in the compressible regime plays a major role in many applications such as aerospace, defense and transportation. Under supersonic flow conditions, thermal effects, including surface and bulk (*i.e.*, gas) heating, are commonly interpreted as the main physical mechanisms responsible for aerodynamic effects resulting from electrical discharges created in the air flow [2, 19]. While many experimental studies have been undertaken at high speed flows, the interpretation of some of the experimental results remains problematic [20-24], especially for experiments in which a change in the discharge polarity leads to different aerodynamic

effects [21, 24]. Analysis of the investigations carried out to date highlights the fact that the results of many studies are attributed to purely thermal effects. In such cases, the flow modifications are due to thermal mechanisms of interaction coming from the energy release of the discharge. However, when the ionization degree is relatively high ($> 10^{-5}$, [25]), other types of effects must be considered to explain the observed flow modifications [26].

The scope of this paper is to analyze the behavior of a glow discharge operating in the abnormal regime to understand how the coupling between the plasma and the flow takes place and induces the modification of the shock wave. This study follows previous works presented in [13, 27, 28], where it was shown that the surface heating of the flat plate surface contributes to the increase in the shock wave angle. For the experimental setup studied in the present work, it is now confirmed that the purely thermal effect at the flat plate surface only accounts for almost half of the total shock wave modification when the plasma actuator is used [28]. This means that surface heating is overlapped with purely plasma effects. Therefore, other properties of the glow discharge than surface and gas heating are considered to explain the observed flow modifications.

This paper presents experiments carried out to gain a better knowledge of the plasma properties of the discharge used to modify the flow around a flat plate. Measurements of electron properties (*i.e.*, temperature and density) with a Langmuir probe are conducted in order to quantify the level of the ionization degree, which is known to have the ability to significantly modify gas properties such as the isentropic exponent γ [29]. In particular, the positions upstream of the leading edge of the flat plate are surveyed, since a necessary condition to achieve a noticeable plasma effect is to alter flow properties upstream the model [30]. A simplified theoretical model is introduced in order to link the plasma properties to the flow ones. This allows the modification of the flow properties by the discharge to be estimated, and shows that the ionization degree has a sufficiently high level to modify the flow properties in the vicinity of the shock wave.

2 EXPERIMENTAL SETUP

2.1 THE MARHY WIND TUNNEL

MARHy is a low density facility located at the ICARE laboratory and used for both academic and industrial researches. This wind tunnel was built in 1963, and until 2006 'MARHy' was known as the 'SR3' wind tunnel of the 'Laboratoire d'Aérothermique' (former name of ICARE). Figure 1 presents a schematic view of the facility presenting the three main parts: the settling chamber with a diameter of 1.3 m and a length of 2.0 m, the test chamber with a diameter of 2.3 m and a length of 5.0 m, and a third chamber in which a diffuser is installed. The diffuser is connected to the pumping group by a vacuum gate. A powerful pumping group with a total capacity of 153,000 m³.h⁻¹ ensures the low density flow conditions in continuous operating mode. When supplied with different nozzles, the wind tunnel generates subsonic, supersonic and

hypersonic flows from Mach 0.8 to Mach 21, and covers a large range of Reynolds numbers from 10^2 up to 10^5, for a reference length of 10 cm. The present study is carried out with a Mach 2 contoured nozzle, giving a uniform flow distribution through the test section with a core of 12 cm in diameter. The nominal operating conditions, detailed in Table 1, are: 63 Pa for the stagnation pressure and 8 Pa for the static pressure of the test section, corresponding to a geometric altitude of 67 km. The subscripts $_0$ and $_1$ stand for the stagnation condition and the free stream one, respectively. The Mach number M_1 of the gas flowing out of the nozzle is defined with the following relation:

$$M_1^2 = \frac{2}{\gamma - 1}\left[\left(\frac{p_0}{p_1}\right)^{\frac{\gamma-1}{\gamma}} - 1\right] \qquad (1)$$

where p_0 is the stagnation pressure, p_1 is the static pressure of the test section, and γ is the isentropic exponent of the flow (for an unionized air, $\gamma = 1.4$).
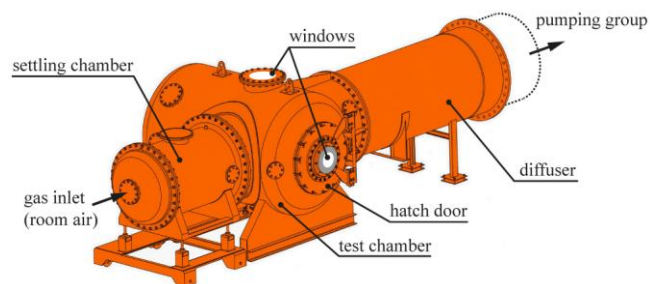

Figure 1. Schematic view of the MARHy wind tunnel without the pumping group.

Table 1. Operating conditions.

Stagnation conditions	Free stream conditions
$p_0 = 63$ Pa	$P_1 = 8$ PA
$T_0 = 293$ K	$T_1 = 163$ K
$\rho_0 = 7.44e^{-4}$ kg.m⁻³	$\rho_1 = 1.71e^{-4}$ kg.m⁻³
	$\mu_1 = 1.10e^{-5}$ Pa.s
	$U_1 = 511$ m.s⁻¹
	$M_1 = 2$
	$\lambda_1 = 0.375$ mm
	$q_m = 3.34e^{-3}$ kg.s⁻¹

2.2 FLAT PLATE AND PLASMA ACTUATOR

A schematic view of the experimental arrangement is presented on Figure 2. The model under investigation is a flat plate mounted in the test section, 174 mm downstream the nozzle exit. The flat plate is made of quartz with 100 mm long, 80 mm wide, and 4 mm thick and presents a sharp leading edge of 15°. The Reynolds number ($Re_L = U_1 \times L / \nu_1$) based on the flat plate length L and calculated with the experimental inflow conditions (Table 1) is $Re_L = 794$. The Knudsen number ($Kn_L = \lambda_1 / L$) based on the same experimental conditions is $Kn_L = 0.004$, corresponding to the slip-flow regime or slightly rarefied regime.
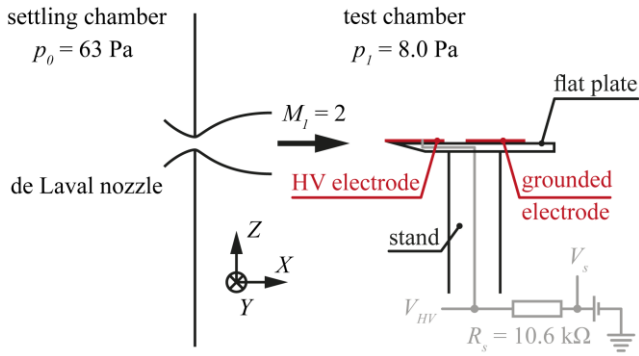
Figure 2. Schematic view of the flat plate with the plasma actuator.

The plasma actuator is composed of two aluminum electrodes (80 mm long, 35 mm wide, 80 μm thick), flush mounted on the upper surface of the flat plate with a gap of 20 mm separating both electrodes (Figure 3). The active electrode is set at the leading edge of the plate and is connected to a high voltage dc power supply (Spellman, SR15PN6) through a resistor (R_s = 10.6 kΩ), while the second one is grounded. The glow discharge is generated with a negative dc potential applied to the active electrode, acting as a cathode. The power supply operates in stabilized voltage mode meaning that the high voltage V_s is fixed and the discharge current I_{HV} depends on the plasma impedance. The voltage applied to the active electrode, V_{HV}, is then calculated with the following relation: $V_{HV} = V_s - R_s \times I_{HV}$. The discharge is ignited in air.
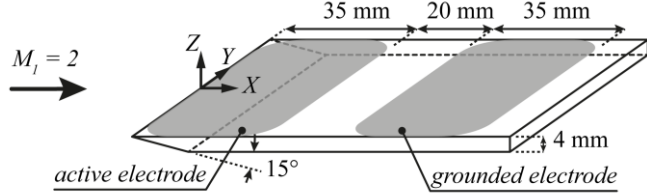

Figure 3. Dimensions of the flat plate with the plasma actuator.

2.3 MEASUREMENT DIAGNOSTICS

2.3.1 PRESSURE MEASUREMENT

The Mach 2 air flow is set by the difference between the settling chamber pressure and the test chamber pressure. To ensure a good operating mode during experiments, the wind tunnel parameters are continuously acquired. Specially the stagnation pressure p_0 and test section pressure p_1 were measured with two MKS Baratron capacitance manometers (Type 627D) with 0-10 Torr and 0-0.1 Torr ranges, respectively. Both manometers are connected to a MKS control unit (PR 4000B) with a 12-bit resolution. According to the information provided by the manufacturer, the 0-10 Torr (0-0.1 Torr) pressure transducer has a signal accuracy of $\Delta p_0^{acc} = \pm 0.12\%$ ($\Delta p_1^{acc} = \pm 0.15\%$) of the reading, and a time response below 20 ms (40 ms).

2.3.2 VISUALIZATION OF THE DISCHARGE

A PI-MAX Gen-II ICCD camera (1024×1024-pixel array)

equipped with a VUV objective lens (94 mm, f/4.1) is used to collect through a quartz window located at the wall of the test section chamber the light emitted from the weakly ionized plasma. Due to the rarefaction level of the flow, the natural flow field around the plate is experimentally visualized through the glow-discharge flow visualization technique. A description of this visualization method can be found in [31]. This technique is applied to analyze the flow field of the natural case (without actuation). When the plasma actuator is used, this technique is not employed because the bright visible emission of the discharge itself allows visualization of the flow around the flat plate and the shock wave.

2.3.3 SURFACE TEMPERATURE MEASUREMENT

An infrared thermography camera is used to measure the surface temperature of the flat plate during experiments when the plasma actuator is switched on. In this study, the thermal images are obtained with a FLIR ThermaCAM SC3000 camera. The spectral range of the IR camera lies between 8 μm and 9 μm. The IR camera is placed on top of the wind tunnel and focused the entire surface of the flat plate through a fluorine window (CaF_2), compatible with the IR wavelength range of the camera. The camera is equipped with a QWIP-type IR photo-detector composed of a 320×240-pixel array, cooled down at 70 K by a Stirling cryocooler. For each experimental case, the temperature measurements are performed once thermal equilibrium had been reached (≈15-20 min, [32]). The surface temperature along the flat plate is obtained by post-processing 100 images recorded at 1 Hz with the IR camera. The emissivity of the flat plate surface is determined using the direct emissivity measurement method [33]. This consists in measuring locally the surface temperature simultaneously with both the IR camera (T_{cam}) and a K-type thermocouple flush mounted on the flat plate surface.

2.3.4 MEASUREMENT OF ELECTRON DENSITY AND TEMPERATURE

Since the pioneering work of Irvin Langmuir in 1924 [34], electrostatic probes are used as a fundamental diagnostic tool for measuring local properties of the plasma, in particular electron density n_e and electron temperature T_e. Although the electrostatic probe devices are relatively simple, the theory underlying the probe response is rather complicated because probe theories depend on plasma and probes characteristics like the mean free path λ, the probe radius R, and the Debye length λ_D. For the present paper we focus on the collision-less or classical Langmuir probe theory. The validity of using this theory in our flow and discharge conditions will be discussed in Section 5.4.

The Langmuir probe measurements are performed with a single plane probe made with a tungsten wire of circular section (1 mm in diameter) insulated within an alumina tube of 3 mm in external diameter. The probe is mounted vertically on a 3-axis traversing system and is connected to a voltage generator delivering periodic triangular signals with adjustable rise and fall times. In our experiment conditions, the probe measurements are carried out with a

100 Hz bias voltage applied to the tungsten wire. Depending on the plasma properties, various positive and negative bias voltages are tested. The collected probe current is measured through a resistor (100 Ω) adapted to the plasma impedance. Probe signals (current and applied potential) are recorded simultaneously with a digital oscilloscope (Tektronix DPO4034, 350 MHz, 2.5 Gs/s, 8 bits). In this study, a single probe configuration is used, consisting on one small electrode surface (*i.e.*, the tungsten wire) inserted into the plasma.

3 MORPHOLOGY OF THE GLOW DISCHARGE WITHOUT FLOW

To better understand the coupling between the glow discharge and the rarefied flow, we first focus on the analysis of the glow discharge morphology without the Mach 2 flow but with the same static pressure condition. When the high voltage is switched on, gas above the cathode is ionized and a weakly ionized plasma is created. Figure 4 shows an image obtained with the ICCD camera without post-processing (Figure 4a) and with the contrast enhanced with ImageJ program [35] (Figure 4b). The static pressure into the test chamber is set to $p_1 = 8.0$ Pa. The voltage applied to the active electrode is $V_{HV} = -1.43$ kV, giving a discharge current of $I_{HV} = 18$ mA and, hence, a plasma resistance of $R_{HV} = 79.4$ kΩ.
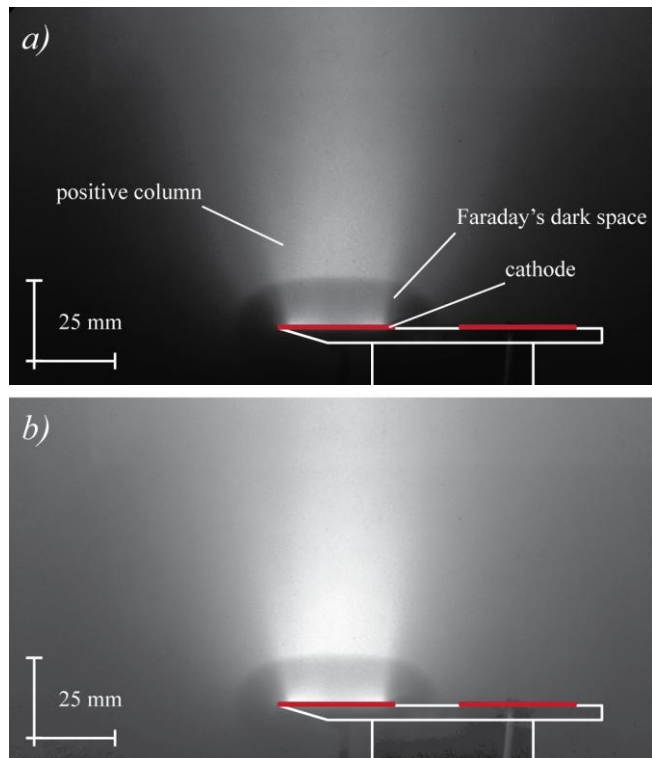

Figure 4. Image of the discharge ($V_{HV} = -1.43$ kV and $I_{HV} = 18$ mA) without flow for a static pressure of $p_1 = 8.0$ Pa: *(a)* raw image, and *(b)* post-processed image (contrast enhancement).

The plasma discharge exhibits a plume-like shape directed in the wall-normal direction, and is divided into three main distinct zones. The first region corresponds to the negative glow, giving to the active electrode (*i.e.*, the

cathode) a glowing aspect. As the thickness of this region is small, typically less than 1 mm, it is very difficult to observe it on Figure 4. The second region is the Faraday's dark space, corresponding to the large oblong-like dark area around the cathode [36]. Without the Mach 2 flow, the Faraday's dark space has a thickness of about 15-20 mm, and then overtakes the leading edge of the flat plate (see Figure 4b). The third region corresponds to that beyond the Faraday's dark space, called the positive column. In comparison to the negative glow and the Faraday's dark space, the positive column is the largest and most homogeneous region and can be detected as the most luminous region. Because the active electrode is flush mounted on the flat plate surface, the plasma is mainly present above this electrode and is directed into the wall-normal direction. In the experimental conditions of this study, the mean free path is rather large in comparison to the electrode gap. Therefore, the charged species are collected by metallic parts of the wind tunnel (grounded), ensuring the current looping, rather than be collected by the downstream electrode, even if this electrode is grounded. At higher static pressure (typically, for $p_1 > 100$ Pa), the discharge morphology changes and the plasma begins to establish between the active electrode and the grounded one.
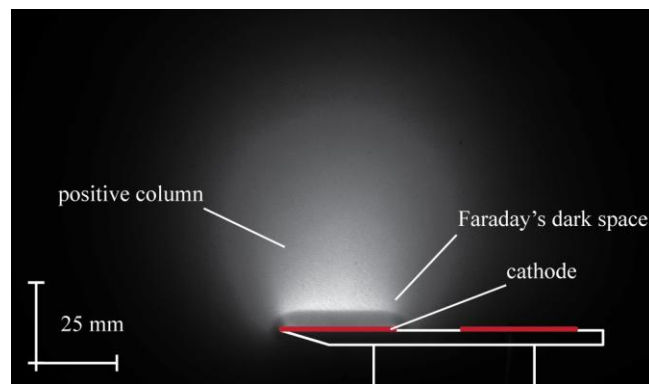

Figure 5. Image of the discharge ($V_{HV} = -0.79$ kV and $I_{HV} = 18$ mA) without flow for a static pressure of $p_1 = 24.0$ Pa; image without post-processing.

The influence of the static pressure on the morphology of the glow discharge has also be studied. Figure 5 shows an image of the discharge with the static pressure set to $p_1 = 24.0$ Pa. The applied voltage is tuned to obtain the same discharge current than those obtained with a static pressure set to $p_1 = 8.0$ Pa. In this case, the applied voltage is decreased ($V_{HV} = -0.79$ kV) to keep constant the current ($I_{HV} = 18.0$ mA). This observed behavior is characteristic of a glow discharge operating in an abnormal regime at a low pressure and is consistent to experimental measurements reported in the literature (for instance, see [37-39]). It corresponds to the fact that collisional processes are more efficient at higher pressure, thus requiring a lower applied voltage to have the same current [40]. As observed, an increase in the static pressure p_1 induces a shrinking of the Faraday's dark space because the mean free path increases with the static pressure. For $p_1 = 8.0$ Pa, the mean free path

λ_{e-N_2} between electrons and nitrogen molecules is $\lambda_{e-N_2} = 1.09$ mm, while it is equal to $\lambda_{e-N_2} = 0.36$ mm for $p_1 = 24.0$ Pa. The mean free path λ_{e-N_2} is calculated in considering a total scattering cross section for electron collisions with nitrogen molecules of $\sigma_{e-N_2}^{tot} = 25.7e^{-16}$ cm^2 [41]. The lower applied voltage contributes also to this shrinkage. In addition, the size of the positive column is smaller in comparison to the case with $p_1 = 8.0$ Pa. These results show that the discharge morphology is strongly affected by the local pressure value of the region around the active electrode.

4 THE BASELINE FLOW FIELD

The flow field around the flat plate is first investigated without the plasma actuator working, corresponding to the study of the natural flow around the flat plate (namely, the baseline flow). In this case, the shock wave is experimentally visualized with the discharge flow visualization technique. Figure 6 shows an image of the baseline flow around the flat plate visualized with the ICCD camera. This image results from the averaging and post-processing of 150 snapshots of the flow field recorded with the ICCD camera. The contrast is enhanced with ImageJ program in order to distinguish the shock wave position more precisely than is possible from the raw image. The air flows from the left to the right.
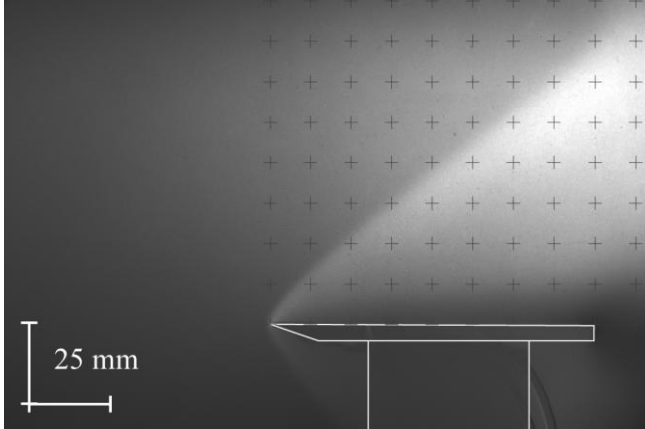

Figure 6. Image of the natural flow field around the flat plate obtained with the glow-discharge flow visualization technique (exposure time of 50 ms). The free stream Mach number is 2.

The shock wave is readily recognized on the image captured with the ICCD camera and its shape obeys to an hyperbola fitted with the following equation:

$$x = c_1 + c_2 \left[1 + \left(\frac{z}{c_3} \right)^2 \right]^{1/2} \qquad (2)$$

where x and z are the shock wave coordinates in the Cartesian coordinate system (centered on the leading edge), and c_1, c_2 and c_3 are the geometric coefficients of the hyperbola. The shock wave angle β corresponds to the angle of the hyperbola asymptote (*i.e.*, the Mach angle). The coefficients c_1, c_2 and c_3 are estimated by fitting (least squares method) the shock wave position on the ICCD images, enabling the shock wave angle to be calculated. For the baseline flow, the value of the shock wave angle is $\beta_{off} = 36.71° \pm 0.68°$. For a given experimental configuration (V_{HV}, I_{HV}), the value of β is obtained by repeating (three times) the analysis of the same series of images. The total uncertainty $\Delta\beta$ is calculated according to [42] in considering a confidence interval of 95% (see [28] for further details). The shock wave is slightly detached from the leading edge of the plate because of the rarefaction effects. The magnitude order of the shock wave stand-off distance is 1-2 mm. For the baseline flow, the longitudinal distribution of the surface temperature measured with the IR camera along the flat plate is homogeneous: T_w ranges between 286.7 K and 288.8 K with an average value of ≈ 287.4 K.
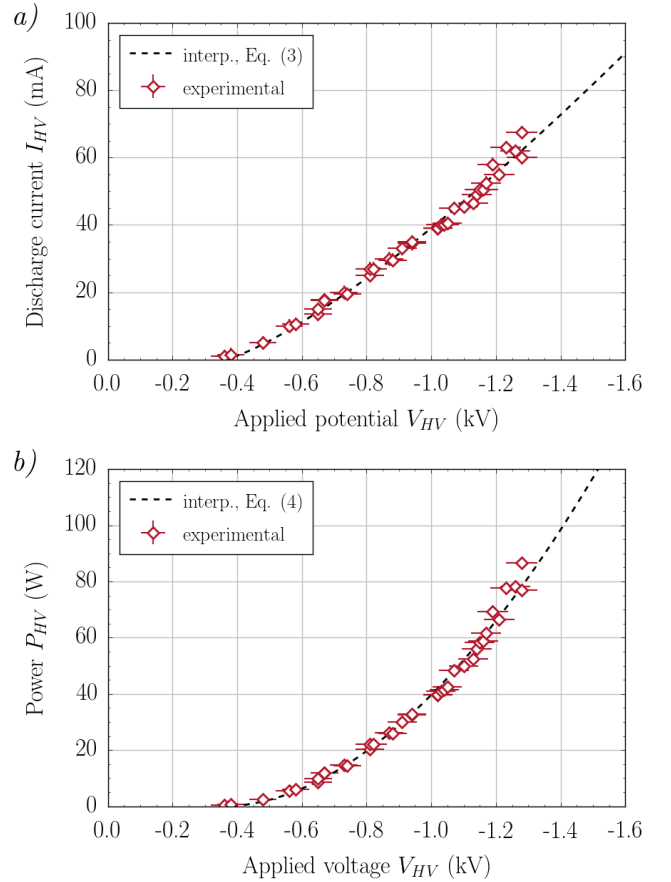

Figure 7. Electrical characterization of the plasma actuator in a Mach 2 air flow: *(a)* current-voltage characteristic and *(b)* power consumption versus the applied voltage. The free stream Mach number is 2.

5 DISCHARGE CHARACTERIZATION IN A RAREFIED MACH 2 FLOW

5.1 ELECTRICAL PARAMETERS

A negative dc potential is applied to the active electrode, generating a glow discharge. Figure 7 shows the current-

voltage characteristic (I_{HV} - V_{HV}). The 2D *xy*-plots were produced in Python, using the NumPy and Matplotlib environment [43, 44]. The error-bars represent the total uncertainty estimated according to [42] and the error propagation law suggested by [45]. The discharge ignites at around $V_{ign} = -0.36$ kV ± 0.01 kV, and can be sustained down to around $V_{HV} \approx -2.5$ kV. Within this range the discharge current increases with the applied voltage as

$$I_{HV} = a\left(V_{ign} - V_{HV}\right)^n, \qquad (3)$$

where V_{ign} is the ignition voltage in kV, and $a = 69.2$ mA.kV^{-n} ± 0.9 mA.kV^{-n} and $n = 1.28$ ± 0.03 are the best-fit parameters with their corresponding standard errors obtained by fitting (least-squares method) the experimental data to a given model. The standard errors of best-fit parameters were calculated with the Python-based Kapteyn package [46] by taking into account errors both in *x* and *y* using the effective variance method (*i.e.*, weighted fits). The shape of the I_{HV} - V_{HV} characteristic is typical of a glow discharge operating in the abnormal regime, for which the current is increased by increasing the applied voltage [36]. The relationship between V_{HV} and I_{HV} (*i.e.*, the values of *a* and *n* in relation (3)) depends on the pressure, the gas, and the discharge configuration (for instance, see [39]). The power consumed by the plasma actuator is estimated with I_{HV} and V_{HV} and evolves as

$$P_{HV} = a\left(V_{ign} - V_{HV}\right)^n \qquad (4)$$

where $a = 91.5$ W.mA^{-n} ± 3.3 W.mA^{-n} and $n = 1.87$ ± 0.08 are the best-fit parameters with their corresponding standard errors. The plasma resistance R_p, calculated from V_{HV} and I_{HV}, is presented in Figure 8. The plasma resistance has a decreasing trend and tends to $R_p \approx 20$ kΩ for high values of the discharge current. This behavior is similar in terms of both value and shape to those reported in the literature. For an abnormal glow discharge at a pressure below 10 Torr, the plasma resistance decreases with the applied voltage, and ranges typically between 10 kΩ and 100 kΩ [38, 39]. The decreasing plasma resistance with the applied voltage is a typical property of such a type of discharge [36], explaining why the voltage-current characteristic (see Figure 7a) has a positive slope (*i.e.*, $n > 1$ in relation (3)).
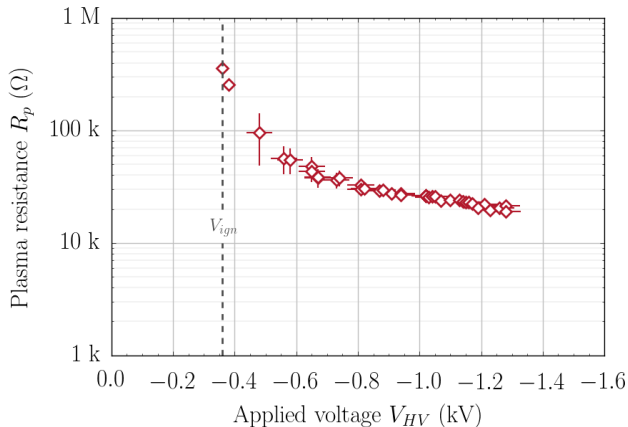

Figure 8. Plasma resistance R_p versus the applied voltage V_{HV}. The free stream Mach number is 2.

5.2 SURFACE TEMPERATURE

As already observed in previous works, one of the plasma actuator effects is the heating of the surface plate inducing a modification of the flow field around the plate [13, 28, 32]. The main contribution to the cathode heating is the bombardment of energetic neutrals and returning ions, in particular positive ions [36]. Because the flat plate is beveled, the electric field is stronger in the vicinity of the leading edge [32]. This non-uniform distribution of the electric field above the cathode induces an intensification of bombardment by ions, and thus an increase in the surface temperature of the cathode in this region. The longitudinal distribution of the surface temperature is therefore not constant along the flat plate, as evidenced by the infra-red camera measurements presented in Figure 9. Over the range of electrical configurations tested with the plasma actuator, the maximum surface temperature $T_{w,max}$ evolves with the applied voltage as a power law [28].
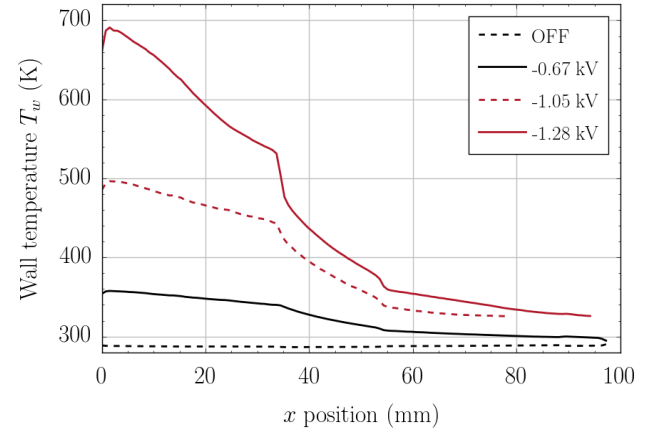

Figure 9. Longitudinal distribution of the surface temperature T_w in the case of the plasma actuator. The free stream Mach number is 2.
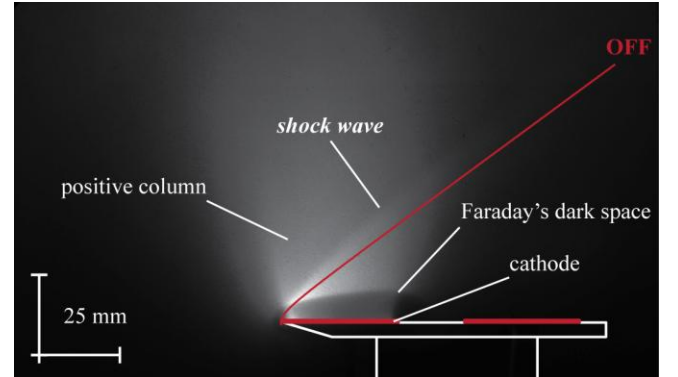

Figure 10. ICCD image of the flow field modified by the plasma actuator ($V_{HV} = -1.44$ kV and $I_{HV} = 37$ mA). The solid line represents the shock wave shape of the baseline flow. The free stream Mach number is 2.

5.3 DISCHARGE MORPHOLOGY

Figure 10 shows an image obtained with the ICCD camera of the flat plate with the plasma actuator operating in a Mach 2 air flow. One can observe that the discharge exhibits the same three distinct regions as those described previously (see Section 3). However, the plasma discharge

exhibits a plume-like shape slightly slanted in the upstream direction. Because a shock wave is present around the flat plate, the Faraday's dark space is slightly slanted in the upstream direction. The Faraday's dark space has a variable thickness, ranged approximately between 5 mm and 15 mm. The thickness depends on the longitudinal position along the flat plate (*i.e.*, along the *X*-axis) because the developing laminar boundary layer induces different wall-normal variations of the pressure (*i.e.*, along the *Z*-axis) [27]. The shock wave position corresponds to the oblique gradient of luminosity observed into the positive column above the flat plate.

5.4 ELECTRON POPULATION ANALYSIS

Measurements of the electron density n_e and temperature T_e of the plasma are performed with a Langmuir probe. For the present study, the analysis is done using the collision-less or classical Langmuir probe theory which implies

$$\lambda_D \leq R \leq \lambda_{e-N_2} \qquad (5)$$

where λ_D is the Debye length, R is the probe radius, and λ_{e-N_2} is the mean free path between neutral and electrons. The electron current is related to the electron density and electron temperature by the following equation

$$I_e(V) = A_s e n_e \left(\frac{k_B T_e}{2\pi m_e} \right)^{1/2} \qquad (6)$$

where m_e is the electron mass and A_s is the probe surface. Nevertheless, the classical Langmuir theory has to be verified afterward in order to check that the Debye length, the Langmuir probe diameter, and the mean free path λ_{e-N_2} satisfy the relation (5). For an electron temperature ranging between 0.2 eV (2321 K) and 2.5 eV (29,010 K), and electron densities varying from 10^8 cm^{-3} to 10^{13} cm^{-3}, the Debye length decreases from 2 mm till 2 μm. The elementary electric charge $q = 1.6022 \times 10^{-19}$ C and the Boltzmann constant $k_B = 1.38065 \times 10^{-23}$ J.K^{-1} are used to express the temperature in eV. The mean free path λ_{e-N_2} estimated for a range of gas temperature of 300-1000 K, and a gas pressure of 8.0 Pa, is ranged between 0.46 cm and 1.54 cm. The comparison between these three parameters is then verified for a large set of plasma parameters, giving confidence on the use of the classical probe theory in our flow and discharge conditions. The plasma is also characterized by the floating potential ϕ_f and the plasma potential ϕ_p. The former is the potential for which the ionic current counterbalances the electron current (*i.e.*, the total current is null), and the latter is obtained from the maximum of the first derivative of the probe characteristic.

The plasma parameters (ϕ_f, ϕ_p, n_e, and T_e) are measured in the vicinity of the cathode, especially in the region upstream the flat plate. Horizontal and vertical probe characteristic profiles have been carried out for -1.13 kV and 30 mA. Results are presented on Figures 11 and 12, respectively.
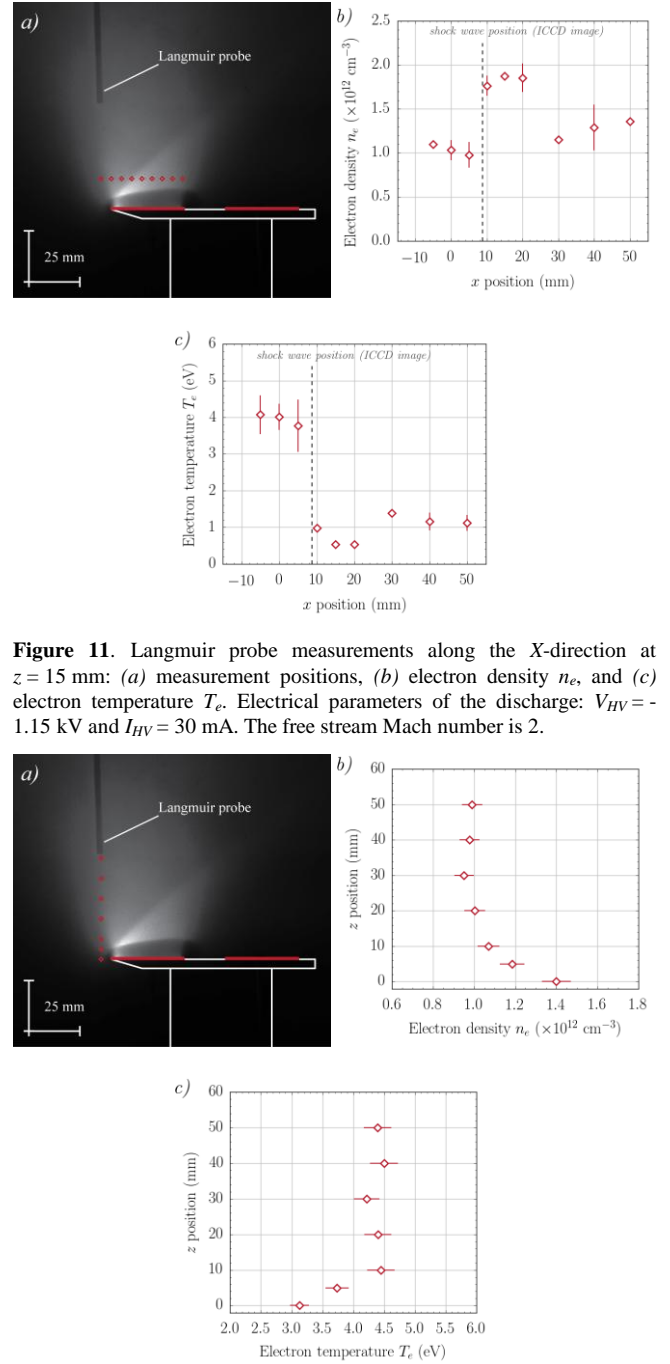

Figure 11. Langmuir probe measurements along the *X*-direction at $z = 15$ mm: *(a)* measurement positions, *(b)* electron density n_e, and *(c)* electron temperature T_e. Electrical parameters of the discharge: $V_{HV} = $ -1.15 kV and $I_{HV} = 30$ mA. The free stream Mach number is 2.

Figure 12. Langmuir probe measurements along the *Z*-direction at $x = $ -5 mm: *(a)* measurement positions, *(b)* electron density n_e, and *(c)* electron temperature T_e. Electrical parameters of the discharge: $V_{HV} = -1.15$ kV and $I_{HV} = 30$ mA. The free stream Mach number is 2.

Even if the measurement positions presented in Figure 12a are located upstream the flat plate, and therefore the cathode, the electric field is strong enough to ionize the flow upstream the model. The electrons have indeed their mobility which obeys to the electric field configuration and not to the density of the heavy particles (*i.e.*, the shock wave). In addition, it may be noticed that the electron density profile presents a maximum at $z = 0$ mm, illustrating the inhomogeneous scattering of the light emitted by the discharge. The electron temperature is ranged between 1 eV

(11,605 K) and 4 eV (46,419 K), showing the strong non-thermal equilibrium state of the flow as the gas temperature remains around 300 K. This point could be of interest to explain the modification of the flow field, since the disequilibrium between electrons and heavy particles (*i.e.*, ions and neutrals) is a key parameter to evaluate the strength of the different thermal transfers [36].
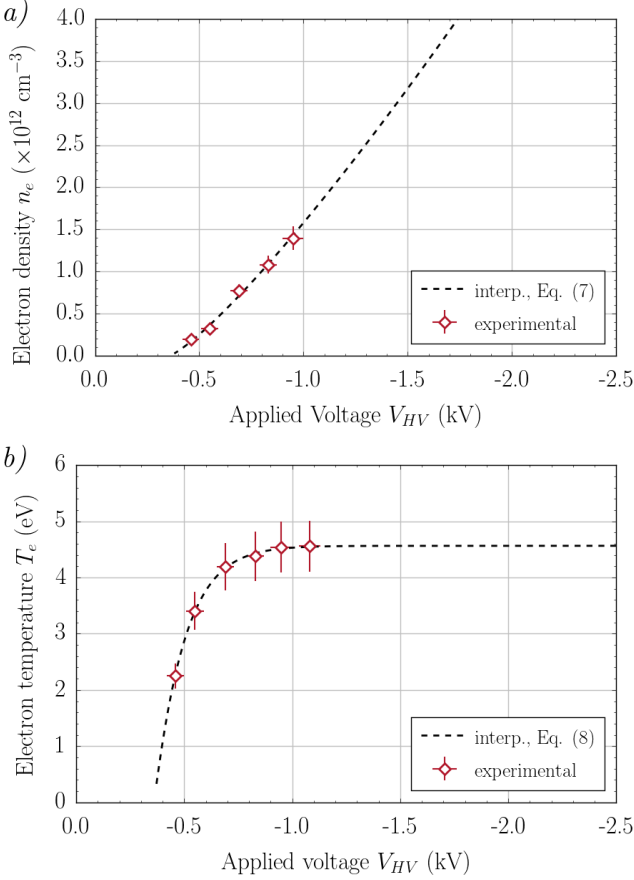

Figure 13. Electron parameters versus the applied voltage, at $x = -5$ mm and $z = 10$ mm: *(a)* electron density, and *(b)* electron temperature. The free stream Mach number is 2.

Figures 13a and 13b show the variation of the electron density n_e and the electron temperature T_e according to the applied voltage, respectively. The measurement position is upstream the flat plate, at $x = -5$ mm and $z = 10$ mm. The increase in the electron density and temperature values with the applied voltage can be described, respectively, by

$$n_e = a\left(V_{ign} - V_{HV}\right)^n \tag{7}$$

and

$$T_e = a\left\{1 - \exp\left[-b\left(V_{ign} - V_{HV}\right)^n\right]\right\} + \frac{qT_1}{k_B} \tag{8}$$

where $a = 2.71\times10^{12}$ cm^{-3}.V^{-1} $\pm0.29\times10^{12}$ cm^{-3}.mA^{-1} and $n = 1.21 \pm0.13$ is the best-fit slope with its corresponding standard error in relation (7), and $a = 4.55$ eV ±0.04 eV, $b = 7.82$ mA ±1.02 mA, and $n = 1.05 \pm1.05$ are the best-fit parameters with their corresponding standard errors in relation (8). The temperature T_1 is expressed in eV in

relation (8) ($T_1 = 0.014$ eV). The increase in n_e with the applied voltage corresponds to a linear increase of the electron density with the discharge current that is consistent with the classical behavior of this type of discharge. The electron temperature has a different behavior. For a discharge current higher than 30 mA, the electron temperature exhibits a plateau and tends to remain constant at $T_e = 4.55$ eV (52,801 K).

From the electron density values one can determine the local ionization degree α_i defined as the ratio of the electron density to the local total density, defined as follows

$$\alpha_i = \frac{n_e}{n_e + n_h} \approx \frac{n_e}{n_h} \tag{9}$$

where n_h is the density of heavy particles which depends on the local pressure (*i.e.*, neutral particles) in m^{-3} and n_e is the electron density in m^{-3}. The ionization degree of the flow upstream the flat plate can be determined from the electron density values of Figure 13 and the local total density of the free stream. At $p = 8.0$ Pa and $T = 162.8$ K, the neutral density is $n_h = 3.56\times10^{21}$ m^{-3}. The variation of the ionization degree with the applied voltage is plotted on Figure 14. It can be observed that for a large part of the applied voltage values experimentally tested, the ionization degree of the plasma upstream the flat plate ranges between 10^{-4} and 10^{-3}. This range is much higher than the one estimated by [47] (1.2-3.0×10^{-7}), for which the shock wave modifications were attributed to only thermal effects.
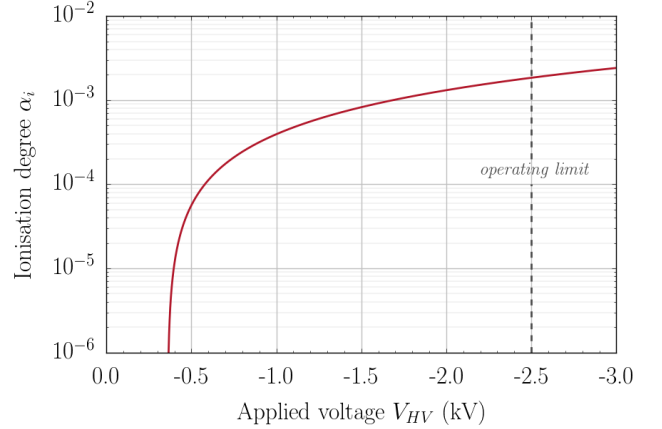

Figure 14. Ionization degree α_i as a function of the applied voltage V_{HV}, at $x = -5$ mm and $z = 10$ mm. The free stream Mach number is 2.

6 ANALYSIS OF IONIZATION DEGREE IN THE SHOCK WAVE ANGLE INCREASE

The plasma discharge induces a modification of the shock wave deflecting it outward from the flat plate surface as illustrated in Figure 10. Figure 15 shows the variation of the shock wave angle with the applied voltage. It can be seen that for higher applied voltage, greater is the increase in the shock wave angle.

In rarefied flow regime, the boundary layer developing over the flat plate surface is thick and then can be affected

by thermal effects, especially those induced by a modification of temperature at the model surface. As a consequence, displacement effects of the boundary layer appear, inducing an increase in the boundary layer thickness, and therefore an increase in the shock wave angle. In the case of the plasma actuator, the glow discharge created above the flat plate surface induces an increase in the surface temperature, leading to a displacement effect experimentally measured [28]. In the case of the baseline flow, $\delta_{99} = 11.7$ mm, whereas $\delta_{99} = 18.7$ mm for a plasma discharge with $V_{HV} = -1.47$ kV and $I_{HV} = 39$ mA, showing the displacement effect induced by the plasma actuator.
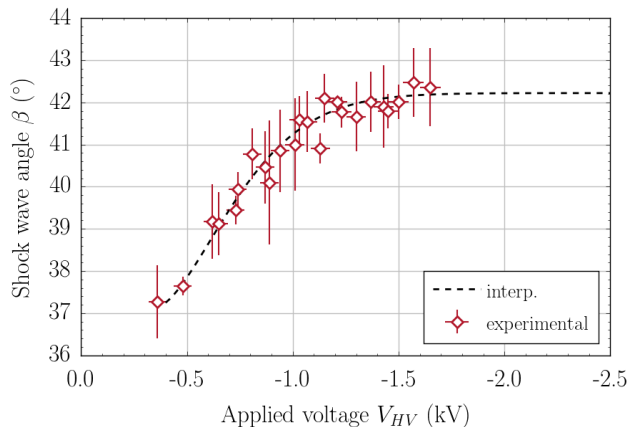

Figure 15. Shock wave angle β versus the applied voltage V_{HV}. The free stream Mach number is 2.

Another possible effect produced by the plasma discharge is bulk heating of the gas above the flat plate surface, inducing an increase in the thermodynamic temperature. This thermal effect has been studied experimentally and numerically with a Monte Carlo simulation [48, 49]. Investigations have shown that bulk heating is too low, an increase of around 10 K is reported, to have an influence on the flow field properties and thus to modify the shock wave angle.

In a previous work [28], the part of the surface heating into the total shock wave angle modification is estimated. Experiments have been carried out with a heating element used instead of the plasma actuator to reproduce the surface thermal effects. It is observed that for the same surface temperature distribution, first the pressure field above a flat plate equipped with a plasma actuator is different to the one obtained with the heating element and secondly that the shock angle increase is also higher with the plasma actuator than with the heating element. It appears that other processes must be considered to fully explain the shock wave modification experimentally measured. In a previous work [26], the authors have shown that a Mach 2 flow field around a cylinder was modified by a plasma actuator placed at the stagnation point on a circular cylinder. In this case, the ionization degree is strong enough to decrease the value of the isentropic coefficient of the gas, leading to an increase in the shock wave stand-off distance. Although the nature of the shock wave is different (weak shock wave in this study, strong one in [26]), the conclusions drawn in [26]

lead us to believe that the ionization degree could play a key role to explain the observed modifications over the flat plate, since the flow conditions are the same and the plasma actuator devices are similar.

From this assumption, measurements of the plasma properties (T_e and n_e) have been achieved with a Langmuir probe in order to estimate the ionization degree induced by the discharge, in the vicinity of the cathode and upstream the model. We think that the shock wave is modified by the upstream flow conditions that are influenced by the ionization of the incoming flow. The vertical profile measured 5 mm upstream to the flat plate leading edge shows that the electron density values are not negligible, since n_e is ranged between 1.0×10^{12} cm^{-3} and 1.4×10^{12} cm^{-3} near the flat plate (see Figure 12). On the contrary, the electron temperature, ranged between 3.0 eV (34,814 K) and 4.5 eV (52,220 K), increases when approaching the flat plate. The longitudinal profile measured at $z = 15$ mm clearly shows the increase in the electron density just over the cathode region with the decrease in the electron temperature (see Figure 11). This behavior denotes first that the electron population has enough energy to ionize the gas flow far from the active electrode, and secondly that the electrons are free to move in the opposite direction of the supersonic flow. These properties of electrons lead to a modification of the nature of the incoming gas flow just before interacting with the flat plate. The modification of the flow results into a change in the isentropic exponent of the gas flow. Indeed, in the case of an ionized gas, the isentropic exponent γ^* of a diatomic plasma in non-local thermodynamic equilibrium is given by [29] as

$$\gamma^* = \frac{c_p^*}{c_v^*} \frac{2\theta + (1-\theta)\alpha_i}{2\theta + (1-\theta)\alpha_i + (1-\alpha_i)\alpha_i} \quad (10)$$

where c_p^* and c_v^* are the heat capacities of the plasma [29], $\alpha_i = n_e / n_h$ is the ionization degree with n_e the electron density and n_h the neutral particle density, and $\theta = T_{gas} / T_e$ is the thermal disequilibrium between the gas temperature T_{gas} and the electron temperature T_e. The ionization energy ε_{ion} used in the calculations of c_p^* and c_v^* corresponds to that of the predominant ionized species N_2^+ (15.7 eV, [50]).

As the isentropic exponent value depends on the electron temperature and the ionization degree, one can evaluate the modified value of γ^* as a function of the applied voltage. Figure 16 shows the theoretical variation of γ^* as a function of the applied voltage V_{HV}. The curve shows a noticeable variation of γ^* with V_{HV}, since its value decreases from 1.4, corresponding to the unionized air (i.e., at $V_{HV} = 0$ kV), down to 1.365 at $V_{HV} = -2.5$ kV. The values corresponding to the experimental configurations tested range between 1.37 and 1.38. The lower isentropic exponent upstream the flat plate has a direct influence on the interaction between the supersonic gas flow and the flat plate and, then, on the shock wave.
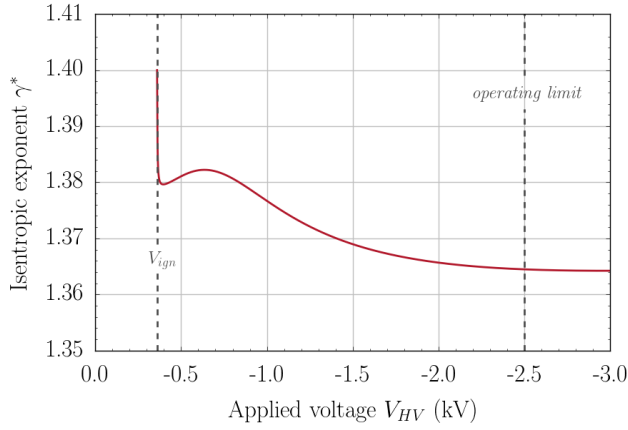
Figure 16. Isentropic exponent γ^* of the plasma upstream the flat plate as a function of the applied voltage V_{HV}, at $x = -5$ mm and $z = 10$ mm. The free stream Mach number is 2.
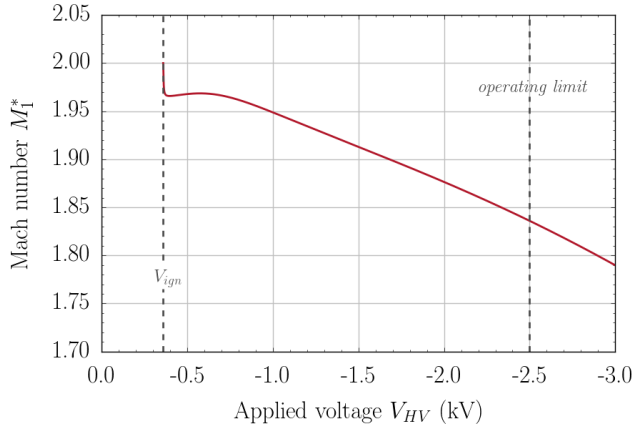

Figure 17. Mach number M_1^* of the plasma flow upstream the flat plate as a function of the applied voltage V_{HV}, at $x = -5$ mm and $z = 10$ mm. The free stream Mach number is 2.

A modification of the isentropic exponent leads to a change in the velocity of the flow and the Mach number [29, 51]. To evaluate this effect we used the Barré de Saint-Venant equation to estimate the flow velocity upstream of the flat plate when the plasma actuator is switched on. This equation can indeed be applied to non-isentropic flows as it is the case in our experimental case with the plasma discharge. This equation can be written as follows

$$\frac{U_1^2}{2} + \frac{c_1^2}{\gamma - 1} = K_1 \qquad (11)$$

where U_1 is the gas flow velocity upstream the flat plate, c_1 is the speed of sound, γ is the isentropic exponent, and K_1 is a constant calculated with the baseline flow conditions. The mass flow conservation law allows the following equation to be written

$$U_1^* = \left[2\left(K_1 - \frac{c_1^{*2}}{\gamma^* - 1} \right) \right]^2 \qquad (12)$$

where U_1^* is velocity of the ionized gas flow, c_1^* is the

modified sound speed in the plasma, and γ^* is the isentropic exponent for the ionized gas flow. Then, the Mach number of the ionized flow M_1^* is determined as the ratio of the flow velocity to the speed of sound calculated with ionized flow conditions. Values are reported on Figure 17 as a function of the applied voltage. As expected, the Mach number decreases when the discharge voltage increases thus when the ionization degree of the gas increases.

With regards to our experimental conditions the Mach number varies from 1.97 and 1.90 over the applied voltage range. As the shock wave angle is proportional to the inverse of Mach number, the decrease in the Mach number due to the lower ionization degree of the gas flow contributes to the increase in the shock wave angle observed experimentally.

7   CONCLUSION

In this study, it is evidenced the influence of the plasma actuator on the modification of the flow field and specially the increase in the shock wave angle. In previous works of our group, it was experimentally observed that the increase in the surface temperature of the flat plate with the applied voltage of the plasma actuator induces an increase in the shock wave angle. Concerning the bulk heating induced by the dc glow discharge, previous works of our group lead us to consider that such a type of heating does not play a significant role in the modification of the rarefied Mach 2 flow field above the flat plate.

This investigation focuses on the analysis of the glow discharge properties that can take part on the flow field modification. The analysis of the glow discharge produced by the plasma actuator without the supersonic flow showed that its morphology depends strongly on the stagnation pressure of the test chamber. As consequence, a strong coupling occurs with the supersonic flow that will have an influence on the interaction between the Mach 2 flow and the flat plate. Measurements with an electrostatic probe are performed and show that, firstly, the glow discharge produces sufficient electron density to modify the gas flow properties and, secondly, that this modification can extend upstream of the flat plate (*i.e.*, in the opposite direction of the Mach 2 flow). The plasma effects result into the modification of properties of the incoming flow before it interacts with the flat plate. In particular, a decrease in the Mach number is expected with the simplified theoretical model proposed in order to explain the increase in the shock wave angle. Future improvements will be considered to gain a better understanding of the coupling between the plasma and the flow.

00078782).

REFERENCES

[1] V. M. Fomin, P. K. Tretyakov, and J.-P. Taran, "Flow control using various plasma and aerodynamics approaches (short review)," Aerosp. Sci. Technol., Vol. 8, no. 5, pp. 411–21, 2004.

[2] P. Bletzinger, B. N. Ganguly, D. van Wie, and A. Garscadden, "Plasmas in high speed aerodynamics," J. Phys. D: Appl. Phys., Vol. 38, No. 4, pp. R33–57, 2005.

[3] S. B. Leonov, "Review of plasma-based methods for high-speed flow control," In: Recent Progresses in Fluid Dynamics Research: Proceeding of the Sixth International Conference on Fluid Mechanics, Guangzhou, China, AIP Conf. Proc., Vol. 1376, pp. 498–502, 2011.

[4] L. Wang, Z. B. Luo, Z. X. Xia, B. Liu, and X. Deng, "Review of actuators for high speed active flow control," Sci. China Tech. Sci., Vol. 55, No. 8, pp. 2225–40, 2012.

[5] E. Moreau, "Airflow control by non-thermal plasma actuators," J. Phys. D: Appl. Phys., Vol. 40, No. 3, pp. R605–36, 2007.

[6] T. C. Corke, C. L. Enloe, and S. P. Wilkinson, "Dielectric barrier discharge plasma actuators for flow control," Annu. Rev. Fluid Mech., Vol. 42, No. 1, pp. 505–29, 2010.

[7] L. N. Cattafesta III and M. Sheplak, "Actuators for active flow control," Annu. Rev. Fluid Mech., Vol. 43, No. 1, pp. 247–72, 2011.

[8] N. Benard and E. Moreau, "Electrical and mechanical characteristics of surface AC dielectric barrier discharge plasma actuators applied to airflow control," Exp. Fluids, Vol. 55, No. 11, p. 1846 (43 pp.), 2014.

[9] M. Kotsonis, "Diagnostics for characterisation of plasma actuators," Meas. Sci. Technol., Vol. 26, No. 9, p. 092001 (30 pp.), 2015.

[10] J. R. Roth, "Aerodynamic flow acceleration using paraelectric and peristaltic electrohydrodynamic effects of a one atmosphere uniform glow discharge plasma," Phys. Plasmas, Vol. 10, No. 5, pp. 2117–26, 2003.

[11] R. Joussot, A. Leroy, R. Weber, H. Rabat, S. Loyer, and D. Hong, "Plasma morphology and induced airflow characterization of a DBD actuator with serrated electrode," J. Phys. D: Appl. Phys., Vol. 46, No. 12, p. 125204 (12 pp.), 2013.

[12] N. Benard, A. Mizuno, and E. Moreau, "A large-scale multiple dielectric barrier discharge actuator based on an innovative three-electrode design," J. Phys. D: Appl. Phys., Vol. 42, No. 23, p. 235204 (12 pp.), 2009.

[13] E. Menier, L. Leger, E. Depussay, V. Lago, and G. Artana, "Effect of a dc discharge on the supersonic rarefied air flow over a flat plate," J. Phys. D: Appl. Phys., Vol. 40, No. 3, pp. 695–701, 2007.

[14] J. S. Shang, R. L. Kimmel, J. Menart, and S. T. Surzhikov, "Hypersonic flow control using surface plasma actuator," J. Propul. Power, Vol. 24, No. 5, pp. 923–34, 2008.

[15] P. Gnemmi and C. Rey, "Plasma actuation for the control of a supersonic projectile," J. Spacecraft Rockets, Vol. 46, No. 5, pp. 989–98, 2009.

[16] S. B. Leonov and D. A. Yarantsev, "Near-surface electrical discharge in supersonic airflow: Properties and flow control," J. Propul. Power, Vol. 24, No. 6, pp. 1168–81, 2008.

[17] G. Artana, J. D'Adamo, L. Léger, E. Moreau, and G. Touchard, "Flow control with electrohydrodynamic actuators," Amer. Inst. Aeronautics Astronautics (AIAA) J., Vol. 40, No. 9, pp. 1773–9, 2002.

[18] J. Dedrick, R. W. Boswell, P. Audier, H. Rabat, D. Hong, and C. Charles, "Plasma propagation of a 13.56 MHz asymmetric surface barrier discharge in atmospheric pressure air," J. Phys. D: Appl. Phys., Vol. 44, No. 20, p. 205202 (8 pp.), 2011.

[19] V. E. Semenov, V. G. Bondarenko, V. B. Gildenburg, V. M. Gubchenko, and A. I. Smirnov, "Weakly ionized plasmas in aerospace applications," Plasma Phys. Contr. F., Vol. 44, No. 12B, pp. B293–305, 2002.

[20] A. Klimov, V. Bityurin, and Y. Serov, "Non-thermal approach in plasma aerodynamics," In: 39th Aerospace Sciences Meeting and Exhibit, Reno, NV, U.S.A., Amer. Inst. Aeronautics Astronautics (AIAA), Paper No. 2001–0348, 2001.

[21] V. A. Bityurin and A. I. Klimov, "Non-thermal plasma aerodynamics effects," In: 43rd AIAA Aerospace Sciences Meeting and Exhibit, Reno, NV, U.S.A., Amer. Inst. Aeronautics Astronautics (AIAA), Paper No. 2005–978, 2005.

[22] S. B. Leonov, D. A. Yarantsev, V. G. Gromov, and A. P. Kuriachy, "Mechanisms of flow control by near-surface electrical discharge generation," In: 43rd AIAA Aerospace Sciences Meeting and Exhibit, Reno, NV, U.S.A., Amer. Inst. Aeronautics Astronautics (AIAA), Paper No. 2005–780, 2005.

[23] J. Shin, V. Narayanaswamy, L. Raja, and N. T. Clemens, "Characteristics of a plasma actuator in Mach 3 flow," In: 45th AIAA Aerospace Sciences Meeting and Exhibit, Reno, NV, U.S.A. Amer. Inst. Aeronautics Astronautics (AIAA), Paper No. 2007–788, 2007.

[24] J. Shin, V. Narayanaswamy, L. Raja, and N. T. Clemens, "Characterization of a direct-current glow discharge plasma actuator in low-pressure supersonic flow," Amer. Inst. Aeronautics Astronautics (AIAA) J., Vol. 45, No. 7, pp. 1596–605, 2007.

[25] S. O. Macheret, M. N. Shneider, and R. B. Miles, "Magnetohydrodynamic and electrohydrodynamic control of hypersonic flows of weakly ionized plasma," Amer. Inst. Aeronautics Astronautics (AIAA) J., Vol. 42, No. 7, pp. 1378–87, 2004.

[26] V. Lago, R. Joussot, and J. D. Parisse, "Influence of the ionization rate of a plasma discharge applied to the modification of a supersonic low Reynolds number flow field around a cylinder," J. Phys. D: Appl. Phys., Vol. 47, No. 12, p. 125202 (13 pp.), 2014.

[27] R. Joussot, V. Lago, and J.-D. Parisse, "Efficiency of plasma actuator ionization in shock wave modification in a rarefied supersonic flow over a flat plate," In: Proceedings of the 29th International Symposium on Rarefied Gas Dynamics, Xi'an, China, AIP Conf. Proc., Vol. 1628, pp. 1146–53, 2014.

[28] R. Joussot, V. Lago, and J.-D. Parisse, "Quantification of the effect of surface heating on shock wave modification by a plasma actuator in a low-density supersonic flow over a flat plate," Exp. Fluids, Vol. 56, No. 5, p. 102 (18 pp.), 2015.

[29] K. T. A. L. Burm, W. J. Goedheer, and D. C. Schram, "The isentropic exponent in plasmas," Phys. Plasmas, Vol. 6, No. 6, pp. 2622–7, 1999.

[30] S. P. Kuo, "Plasma mitigation of shock wave: experiments and theory," Shock Waves, Vol. 17, No. 4, pp. 225–39, 2007.

[31] S. S. Fisher and D. Bharathan, "Glow-discharge flow visualization in low-density free jets," J. Spacecraft Rockets, Vol. 10, No. 10, pp. 658–62, 1973.

[32] L. Léger, E. Depussay, and V. Lago, "D. C. surface discharge characteristics in Mach 2 rarefied airflow," IEEE Trans. Dielectr. Electr. Insul., Vol. 16, No. 2, pp. 396–403, 2009.

[33] W. Minkina and S. Dudzik, Infrared Thermography: Errors and Uncertainties, John Wiley & Sons Ltd, Chichester, United Kingdom, 2009.

[34] I. Langmuir, The collected works of Irving Langmuir: Cloud nucleation. Published with the editorial assistance of the General Electric by Pergamon Press, Vol. 11, 1962.

[35] C. A. Schneider, W. S. Rasband, and K. W. Eliceiri, "NIH Image to ImageJ: 25 years of image analysis," Nat. Methods, Vol. 9, No. 7, pp. 671–5, 2012.

[36] Y. P. Raizer, Gas Discharge Physics, Springer-Verlag, Berlin Heidelberg, 1991.

[37] R. A. Bosch and R. L. Merlino, "Sudden jumps, hysteresis, and negative resistance in an argon plasma discharge. I. Discharges with no magnetic field," Beitr. Plasmaphys., Vol. 26, No. 1, pp. 1–12, 1986.

[38] D. Fang and R. K. Marcus, "Parametric evaluation of sputtering in a planar, diode glow discharge-I. Sputtering of oxygen-free hard copper (OFHC)," Spectrochim. Acta B, Vol. 43, No. 12, pp. 1451–60, 1988.

[39] V. A. Lisovskiy and S. D. Yakovin, "Experimental study of a low pressure glow discharge in air in large-diameter discharge tubes: I. conditions for the normal regime of a glow discharge," Plasma Phys. Rep., Vol. 26, No. 12, pp. 1066–75, 2000.

[40] B. Chapman, Glow Discharge Processes: Sputtering and Plasma Etching, Wiley-Interscience, 1980.

[41] Y. Itikawa, "Cross sections for electron collisions with nitrogen molecules," J. Phys. Chem. Ref. Data, Vol. 35, No. 1, pp. 31–53, 2006.

[42] R. B. Abernethy, R. P. Benedict, and R. B. Dowdell, "ASME measurement uncertainty," J. Fluid. Eng.-T. ASME, Vol. 107, No. 2, pp. 161–4, 1985.

[43] J. D. Hunter, "Matplotlib: A 2D graphics environment," Comput. Sci. Eng., Vol. 9, No. 3, pp. 90–5, 2007.

[44] T. E. Oliphant, "Python for scientific computing," Comput. Sci. Eng., Vol. 9, No. 3, pp. 10–20, 2007.

[45] S. J. Kline and F. A. McClintock, "Describing uncertainties in single sample experiments," Mech. Eng., Vol. 75, No. 1, pp. 3–8, 1953.

[46] J. P. Terlouw and M. G. R. Vogelaar, Kapteyn Package, version 2.2, Kapteyn Astronomical Institute, University of Groningen, The Netherlands, apr 2012, available from http://www.astro.rug.nl/software/kapteyn/

[47] P. Palm, R. Meyer, E. Plönjes, J. W. Rich, and I. V. Adamovich, "Nonequilibrium radio frequency discharge plasma effect on conical shock wave: M = 2.5 flow," Amer. Inst. Aeronautics Astronautics (AIAA) J., Vol. 41, No. 3, pp. 465–9, 2003.

[48] E. Menier, Influence d'une décharge électrique continue sur un écoulement supersonique raréfié, Ph.D. dissertation, Université d'Orléans, France, 2007.

[49] V. Lago, J. C. Lengrand, E. Menier, T. G. Elizarova, and A. A. Khokhlov, "Physical interpretation of the influence of a DC discharge on a supersonic rarefied flow over a flat plate," In: Proceedings of the 26th International Symposium on Rarefied Gas Dynamics, Kyoto, Japan, AIP Conf. Proc., Vol. 1084, pp. 901–906, 2008.

[50] P. Laborie, J. M. Rocard, and J. A. Rees, "Electronic cross-sections and macroscopic coefficients - Metallic vapours and molecular gases", Dunod, Paris, France, 1971.

K. T. A. L. Burm, W. J. Goedheer, and D. C. Schram, "Mach numbers for gases and plasmas in a convergent-divergent cascaded arc," Phys. Plasmas, Vol. 6, No. 6, pp. 2628–35, 1999.

Romain Joussot obtained his Master's degree in Physics and Applications from the Univ. of Orléans (France) in 2007 and received his Ph.D. in Plasma Physics in 2010 from the same institution. Since 2013, he has been working as a postdoctoral fellow at ICARE (CNRS) in Orléans. His research interests include experimental investigations on flow control by plasma actuators. His current studies involve the study of various types of discharges applied to subsonic flows and supersonic rarefied flows.

Viviana Lago holds the position of Research Engineer since 1996 at the CNRS at the Laboratoire d'Aérothermique and then at ICARE in Orléans where she is the scientist manager of the 'Fast' platform: Facilities for Aerothermo-dynamics and Supersonic Technologies. She graduated from Paris XI University in Fundamental Physics in 1990. She obtained the Ph.D. in 1993 from the Université Paris XI, Orsay specialized in 'Gas and Plasmas Physics', and the Research Habilitation Degree in 2013 at the Univ. of Orléans. Her research fields concern experimental investigations on: plasma physics, rarefied gas dynamics, re-entry and hypersonic aerodynamics, thermo-chemical non-equilibrium flows and high-temperature thermo-chemistry and plasma flow control applied to super/hypersonic flows. She is a member of the 3AF Aerodynamic Committee and a member of the 3AF 'Groupe Régional Centre'.